A pediatric brain structure atlas from T1-weighted MR images

Zuyao Y. Shan*[a], Carlos Parra[b], Qing Ji[a], Robert J. Ogg[a], Yong Zhang[a], Fred H. Laningham[c], Wilburn E. Reddick[a,b]

[a]Division of Translational Imaging Research, Department of Radiological Sciences, St. Jude Children's Research Hospital, Memphis, Tennessee 38105, USA; [b] Department of Biomedical Engineering, The University of Memphis, Memphis, TN 38152, USA; [c]Division of Diagnostic Imaging, Department of Radiological Sciences, St. Jude Children's Research Hospital, Memphis, Tennessee 38105

ABSTRACT

In this paper, we have developed a digital atlas of the pediatric human brain. Human brain atlases, used to visualize spatially complex structures of the brain, are indispensable tools in model-based segmentation and quantitative analysis of brain structures. However, adult brain atlases do not adequately represent the normal maturational patterns of the pediatric brain, and the use of an adult model in pediatric studies may introduce substantial bias. Therefore, we proposed to develop a digital atlas of the pediatric human brain in this study. The atlas was constructed from T1 weighted MR data set of a 9 year old, right-handed girl. Furthermore, we extracted and simplified boundary surfaces of 25 manually defined brain structures (cortical and subcortical) based on surface curvature. Higher curvature surfaces were simplified with more reference points; lower curvature surfaces, with fewer. We constructed a 3D triangular mesh model for each structure by triangulation of the structure's reference points. Kappa statistics (cortical, 0.97; subcortical, 0.91) indicated substantial similarities between the mesh-defined and the original volumes. Our brain atlas and structural mesh models (www.stjude.org/BrainAtlas) can be used to plan treatment, to conduct knowledge and model-driven segmentation, and to analyze the shapes of brain structures in pediatric patients.

Keywords: brain atlas, brain structural models, MR images, segmentation

1. INTRODUCTION

Originally, human brain atlases were available only in print form. More recently, digital atlases based on MR images have been developed. Atlases based on MR images provide more useful information than do anatomy books in activities such as the planning of neurosurgical interventions, because the medical team can visualize the brain three-dimensionally, because data are available electronically, and because anatomic shape is based on in vivo images rather than fixed-brain slices[1]. Digital atlases are also indispensable in automated model-based or knowledge-driven brain structure delineations. Because of these advantages, researchers have been very keen to develop atlases (including atlases of probabilistic tissue and brain structures) based on digital images. Studies of atlases of brain tissues were not reviewed here because we focused on anatomic atlases of brain structures. Several atlases of human brain structures based on MR images have been developed for different applications, for example, an early digital three-dimensional brain atlas that was commercially available for the teaching of neuroanatomy[2-4]. Because this atlas was intended primarily for teaching, it was relatively difficult to use interactively, and the data set from which the atlas was constructed was not accessible for further development. Furthermore, the images that were used had been derived from a patient with localized pathology[5]. Also available commercially was a computerized brain atlas developed specifically for brain mapping[6]. For use in surgical planning, Ganser et al. developed a Win32 program that permits the convenient and fast application of standardized anatomy to individual brains[1]. Researchers at the Surgical Planning Laboratory at Brigham and Women's Hospital (Boston) developed a web-interactive and highly detailed brain atlas, which was very good for visualizing brain structures (http://splweb.bwh.harvard.edu:8000/pages/papers/AnatomyBrowser/current/).

One of the most prominent example of brain atlases would be the one that will be constructed by the International Consortium for Brain Mapping a collaborative project developed by several groups. In the final product of this project, a human brain atlas will be constructed from MR images, CT data, and post mortem frozen sections sliced with giant cryomicrotoms. Although the labor intensive labeling is not finished yet, the consortium has provided an anatomic

* zuyao.shan@stjude.org; phone 1 901 495-2673; fax 1 901 495-4398; http://www.stjude.org.

Medical Imaging 2006: Visualization, Image-Guided Procedures, and Display,
edited by Kevin R. Cleary, Robert L. Galloway, Jr., Proc. of SPIE Vol. 6141, 614126, (2006)
1605-7422/06/$15 · doi: 10.1117/12.651922

template based on the MR images of a single subject (www.loni.ucla.edu/ICBM). There are several other brain atlases[5,7-12] have been developed, they do not differ significantly from those discussed above.

Many atlases have been developed for different applications; however, to the best of our knowledge, no digital atlas of pediatric brain structures has been available until now. Such an atlas is needed because the human brain continues to develop throughout childhood and adolescence[13] and the use of an adult template in pediatric neuroimaging studies may introduce significant bias[14].

By using the MR images of a normal child, we have constructed a digital atlas of the structures of the human brain. Twenty-five brain structures were manually delineated: left and right (L/R) frontal lobe, L/R parietal lobe, L/R temporal lobe, L/R occipital lobe, L/R cerebellum, L/R insula, brain stem, L/R amygdala, L/R caudate, cingulate cortex, corpus callosum, L/R hippocampus, L/R putamen, L/R thalamus. This pediatric atlas is specifically designed for model-based segmentation to aid in the planning of surgical and radiation procedures. Therefore, the atlas was further developed into triangulated mesh models, and the complete atlas was made publicly available on the Internet.

2. METHODOLOGY

2.1. MR Image

We selected a three-dimensional T1-weighted MR image of a white, 9-year old, right-handed girl from among those of a control group for another study. The MR imaging had been conducted under an approved protocol and with written informed consent from the patient, parent, or guardian, in accordance with guidelines of the St. Jude Institutional Review Board, the National Cancer Institute, and the Office for Human Research Protection. Retrospectively using the MR data for our study has been approved by our Institutional Review Board.

The MR data were acquired by using a 1.5-T Symphony (Siemens Medical System, Iselin, NJ) whole-body imager with the standard circular polarized volume head coil. A three-dimensional MPRAGE T1-weighted sequence was used. Sagittal images were acquired by using the following imaging parameters: TR = 1800 ms, TE = 2.74 ms, flip angle = 15˚, FOV = 210 mm ? 210 mm, number of slices (contiguous) = 128, slice thickness = 1.25 mm, and matrix = 512 ? 512.

We spatially aligned the MR images to a pediatric template by using an affine registration based on mutual information. The pediatric brain template, constructed from MR images of 200 healthy children, was available from Cincinnati Children's Hospital Medical Center (www.irc.cchmc.org)[14]. Templates are available for three age groups: young children (aged 5-9.5 years old), older children (aged 9.6-12.9 years old), and adolescents (aged 13-18.8 years). We used the pediatric template of young children. Finally, we resampled the MR images into isotropic voxels of 1 mm × 1 mm × 1 mm by using a trilinear algorithm.

2.2. Brain Structure Delineation

Brain structures were manually delineated by an experienced investigator with the help of anatomic books[15-17], previous reports[18-20] and web-based interactive atlases of adult brains (www9.biostr.washington.edu/da.html and splweb.bwh.harvard.edu:8000/). The custom in-house software package used to delineate the structures allowed us to draw structures on saggital and transverse slices and to view them in three orthogonal slices simultaneously. All 25 brain structures were then reviewed by an experienced radiologist (FHL) for accuracy, and modified where necessary.

Left and right hemispheres were divided by the longitudinal fissure. Boundaries for subcortical structures were identical to those described in the references. However, white matter (WM) was included in the lobe segmentation, resulting in boundaries that differ slightly from those previously reported. Our rationale for including the WM in lobe segmentation will be addressed in the Discussion.

Frontal Lobe. The boundaries for the frontal lobe were defined as follows. The lateral and anterior boundaries were defined by the natural limits on every image section. On sections of the superior surface where the central sulcus intersects the longitudinal fissure, the posterior boundary was set at the central sulcus. The inner boundary was defined by the longitudinal fissure (Fig. 1a). On sections that are inferior to the ones listed above, but superior to the sections

containing ventricles, the posterior boundary were central sulcus and a vertical imaginary plane that connected the end of central sulcus and the longitudinal fissure or cingulate cortex. The inner boundary was defined as the longitudinal fissure or cingulate cortex (Fig. 1b). On sections that are inferior to the ones listed above, but superior to the sections containing insula, boundaries were similar to those in the previous sections except where the corpus callosum or ventricle starts. In these sections, the inner boundary was defined by the longitudinal fissure, cingulate cortex, corpus callosum, and ventricle (Fig. 1c). On sections containing the insula, the inner and posterior boundaries were defined by the insula, an imaginary plane that connected the anterior tip of the insula and the posterior tip of the corpus callosum, the cingulate cortex, and the longitudinal fissure (Fig1. d-g).

Parietal Lobe. The parietal lobe (PL) was defined by using the following boundaries: The anterior boundary was defined by the central sulcus and an imaginary plane that dropped vertically from the end of the central sulcus (Fig. 1b, c, and d). The superior boundary was defined by the natural limit on every image section. The inferior boundary was defined by the lateral sulcus and an imaginary plane that extended horizontally from the point where the lateral sulcus changes from a horizontal to a vertical orientation (Fig. 1e). The posterior boundary was defined by the parietal-occipital sulcus (Fig 1. b and c) and an imaginary plane that projected from the superior tip of the parietal-occipital sulcus to the preoccipital notch on image sections where the parietal-occipital sulcus disappears (Fig 1. d-f). Because the preoccipital notch was very difficult to identify on the MR image, we used the posterior tip of the inferior temporal gyrus as an approximation of its location. The inner boundary of the PL was defined by the longitudinal fissure (Fig. 1a), cingulate cortex (Fig. 1b), ventricle and corpus callosum (Fig. 1c), and the insula and an imaginary plane that projected from the posterior tip of the insula to the ventricle (Fig. 1d).

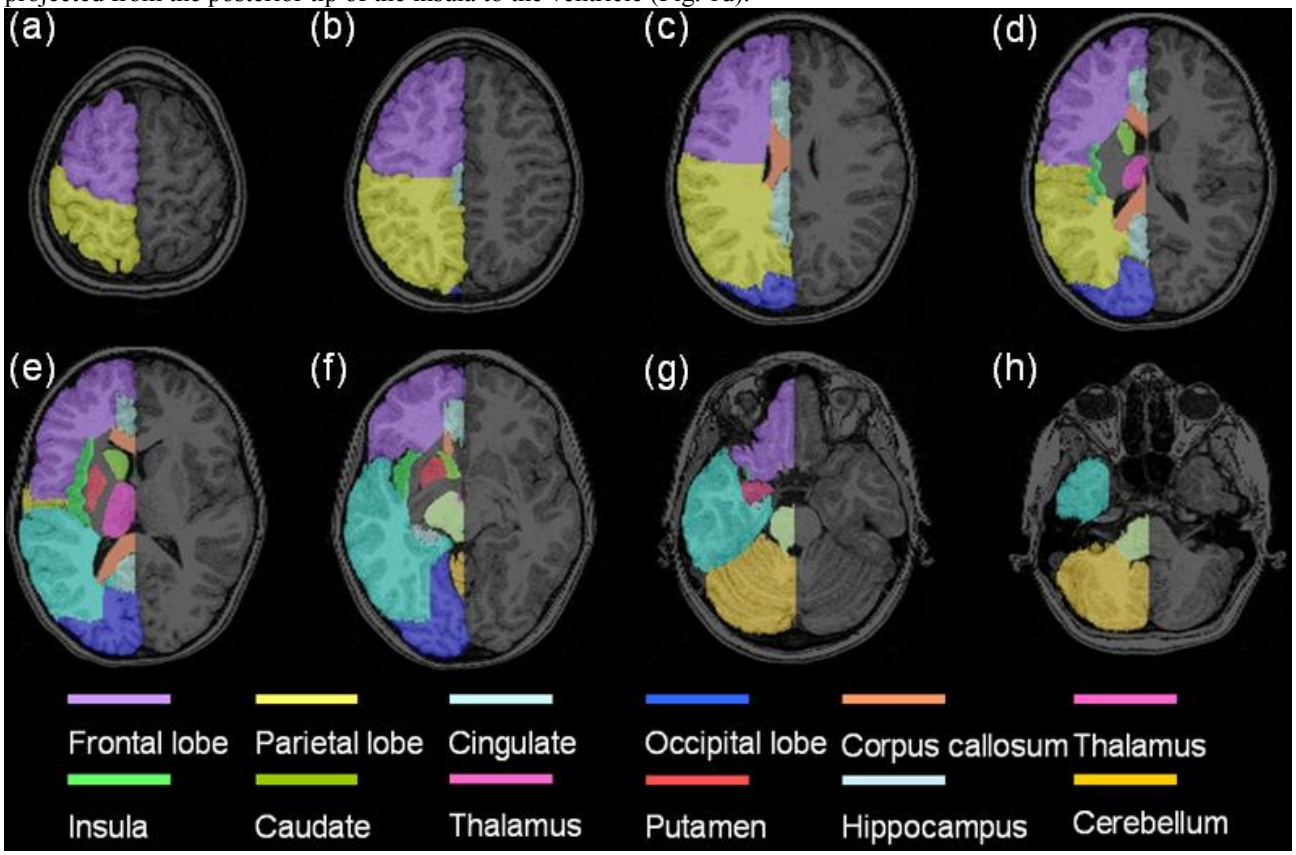

Figure 1: Manual delineation of brain structures. The manually defined volumes of interest are illustrated on selected transverse slices, although the structures were traced on sagittal or transverse slices, depending on which ones were easier to trace. The representative slices are selected from 256 continuous slices, and the structures on the left hemisphere were selected for illustration purpose.

Temporal Lobe. The temporal lobe was defined by using the following boundaries. The superior and posterior boundaries were defined by the inferior boundary of the PL described above. The inner boundary was defined by the insula, an imaginary plane that projected from the posterior tip of the insula to the ventricle (Fig. 1e), the ventricle, the corpus callosum, and the hippocampus. The inferior boundary was defined by the natural limit within each imaging section.

Occipital Lobe. The occipital lobe was defined by using the following boundaries. The anterior boundary was defined by the posterior boundary of the PL described above. The superior, posterior, and inferior boundaries were defined by the natural limit within each imaging section.

2.3. Triangular Mesh Models

The manually defined structures were further developed into individual triangulated mesh models. The boundaries of structures were extracted by using a 26-member neighborhood. A voxel with one or more background voxels within its neighborhood was defined as a boundary voxel. The boundaries were then simplified on the basis of the surface curvature. The boundaries for each structure were scanned in order (X, Y, and Z coordinates). The first voxel encountered was defined as the vertex of the boundaries and as the first focal point. For each focal point, the other boundary points (N = N – {s}) were first divided into groups of neighborhoods with different radiuses (r_i) defined by the Euclidean distance from points in the neighborhood to the focal point. Then, beginning with the group that has the smallest radius, if the difference between the directions of the norms within the group with a radius of r_i was larger than 0.62 (which means that the angle between any pair of norms is smaller than 0.9 radians), all points in this group were removed (boundary points N were updated here, $N = N - N_g$) and the group with a radius of r_{i+1} was evaluated. If the difference between the directions of the norms within the group was equal to or smaller than 0.85, the point with the smallest X, Y, and Z coordinates in this group was selected as the next focal point. These steps were repeated until a focal point was reached that had no neighbors (N = Ø), regardless of the distance. The difference between the direction of the norms within the group was calculated as:

$$\mathbf{n} = Min\left[\frac{(\overrightarrow{sn_i}\times\overrightarrow{sn_j})\bullet(\overrightarrow{sn_i}\times\overrightarrow{sn_k})}{\left\|\overrightarrow{sn_i}\times\overrightarrow{sn_j}\right\|\ \left\|\overrightarrow{sn_i}\times\overrightarrow{sn_k}\right\|}\right] \qquad i,k=1,2,...m \tag{1}$$

where s is the focal point, and n_i, n_j, and n_k are points in this group.

The simplified reference points were then triangulated by using a process similar to the Voronoi graph method[21]. All reference points were expanded simultaneously along the original surface. As the regions of each reference point increased in size, the borders started to collide. The fringe collision of two reference points meant that these two points had the shortest surface distance in this specific direction because all points expanded simultaneously. Therefore, they were connected with each other in a Delaunay triangulation. With the point connection information, we then constructed the triangle mesh of these reference points.

2.4. Model Validation

To evaluate how well the triangular mesh models represented the true structures, we filled the meshes by using a bilinear interpolation algorithm. With the rendered boundary surface, we then defined the volumes of structures. The similarities between mesh-defined volumes and manually delineated volumes were evaluated by calculation of a kappa index for each individual structure model:

$$\kappa(S_a,S_b) = \frac{2\left|S_a \cap S_b\right|}{\left|S_a\right| + \left|S_b\right|} \tag{2}$$

where S_a refers to the structure defined by the mesh models and S_b refers to the manually delineated structure.

3. RESULTS

Figure 1 clearly demonstrates the dependencies, relationships, and positioning of boundary conditions defined for each of the 25 cortical and subcortical regions. A semi-transparent surface rendering of these manually delineated brain

structures is provided in Figure 2. These manually delineated structures formed the basis for the individual triangular mesh models. After validation and refinement of these models by the neuroradiologist (FHL), we generated the triangular mesh models as shown in Figure 3. We then visually inspected the resulting triangular mesh models to check the validity of node assignment and triangle formation as representative of the true surface, which had been manually delineated.

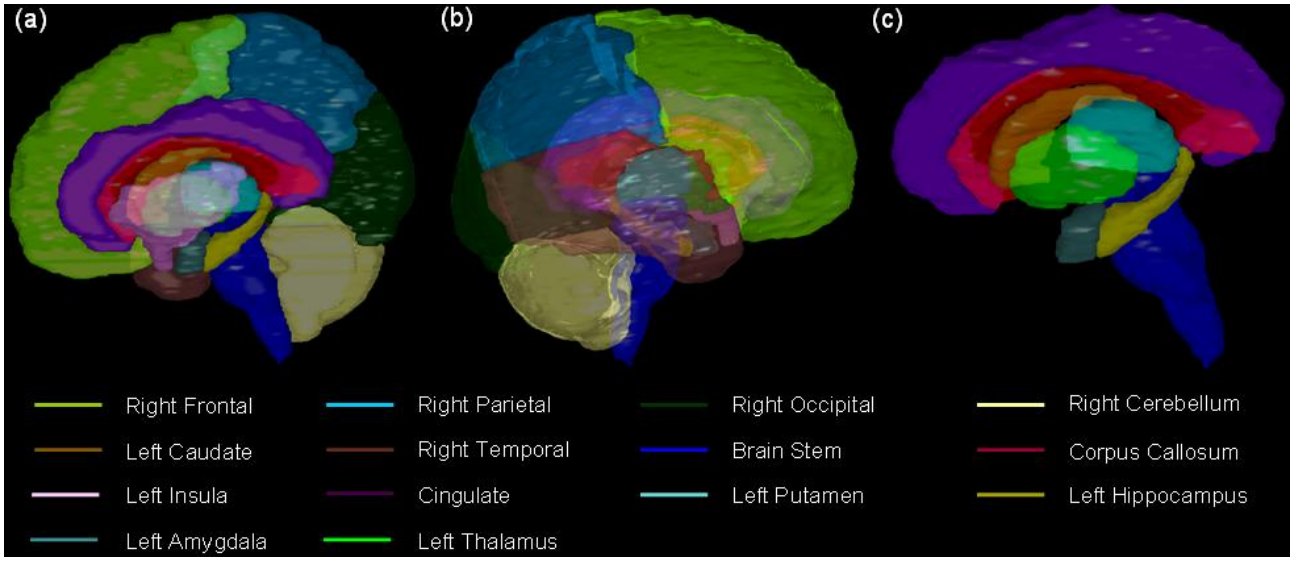

Figure 2: Semitransparent surface of manually defined brain structures. The structures on either hemisphere were selected for illustration purposes. (a) Right lateral view with all structures. (b) Left lateral view with all structures. (c) Right lateral view with subcortical structures (insula was excluded to make it easier to see the putamen and thalamus).

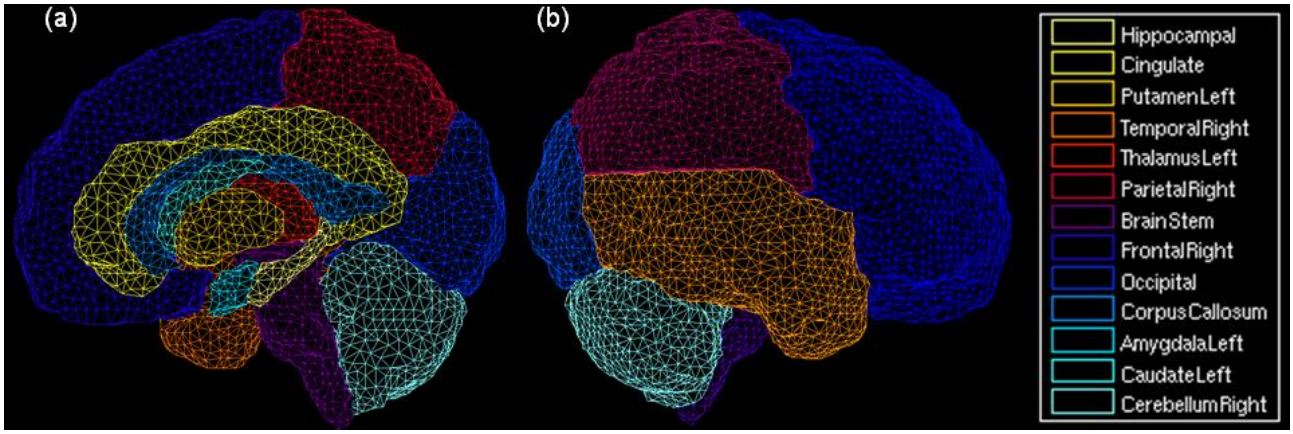

Figure 3: Triangular mesh models of brain structures. The structures on either hemisphere were selected for the purpose of illustration. (a) Right lateral view with all structures. (b) Left lateral view with all structures.

After the triangular models had been generated for each of the brain structures, the similarities between manually defined structures and models were assessed by calculation of the kappa statistic. The average kappa index for cortical structures (frontal lobe, parietal lobe, temporal lobe, occipital lobe, cerebellum, and brain stem) was 0.97, and it ranged from a low of 0.92 in the brain stem to 0.98 or 0.97 in all other cortical regions. The average kappa index for the subcortical structures (amygdale, caudate, hippocampus, thalamus, insula, putamen, cingulate cortex, and corpus callosum) was 0.91, and it ranged from a low of 0.87 in the hippocampus to highs of 0.95 in the thalamus and cingulate cortex.

4. DISCUSSION

Although many adult brain atlases have been developed for different applications, to the best of our knowledge, ours is the first digital pediatric brain atlas. It is based on T1-weighted MR imaging of a normal healthy child. A pediatric brain atlas is necessary because the brain continues to develop throughout childhood and adolescence[13] and because pediatric and adult brain templates and tissue probability maps differ considerably from one another[14], which lead to structural differences.

Even within the pediatric population the brain changes considerably with age[14], we plan to construct two more pediatric brain atlases. So that the brain atlases can be aligned to the corresponding childhood template before manual delineation, we will use the age divisions first suggested by Wilke et al (2003): young children (aged 5-9.5 years), older children (aged 9.6-12.9 years), and adolescents (aged 13-18.8 years).

We have included WM in lobes during manual tracing of the brain although anatomic textbooks define lobes as gray matter[16]. Our rationale was two-fold. First, if future studies required exclusion of WM in lobes, WM could be automatically removed by tissue segmentation methods. In contrast, manually tracing the WM/GM convolution would have been a tedious procedure and one prone to error. Second, WM is generally associated with specific lobes during the planning of radiation therapy and neuroimaging studies. WM tissue is made up of fibers that convey impulses to and from lobes (projection fibers), between different lobes (association fibers), and within the same lobe in the contralateral hemisphere (commissural fibers). The inclusion of WM in the definition of lobes does not consider the integrity of WM fibers; however, it does provide a rough estimation of WM fibers associated with individual lobes.

Because of the inclusion of the WM, the interior boundaries of lobes defined for our atlas differ from those described in previous studies and anatomic books. On the slices superior to the ventricle systems, we used the cingulate cortex and corpus callosum as the interior boundaries of the lobes (Fig. 1, b and c). The cingulum contains fibers that connect regions of the frontal and parietal lobe with parahippocampal and adjacent temporal cortical regions[16]. The corpus callosum reciprocally interconnects broad regions of the cortex in all lobes with the corresponding regions on the contralateral hemisphere. Therefore, WM between a lobe and these two structures should be the WM associated with this specific lobe although the integrity of WM fibers is not considered here. For a similar reason, the interior boundaries of lobes on sections with ventricles were extreme, external, and internal capsules (Fig. 1 d, e, and f). An advantage of this classification is that the entire brain is divided into different structures, with a small portion of unclassified regions, which are made up primarily of extreme, external, and internal capsules. In this way, WM was roughly divided into WM associated with a specific lobe, WM that connects different regions (cingulate cortex), WM that interconnects two hemispheres (corpus callosum), and WM that connects all lobes with subcortical structures (unclassified regions).

A major application of this atlas would be in knowledge-based brain structure segmentation and shape analysis. Therefore, we further developed the atlas into trianglular mesh models. The similarity measures of the models' representation of cortical structures were higher than those of subcortical structures. These differences were caused by the volume size of the structures, i.e., a voxel difference for a model of a small structure would lead to a larger relative error than that of a larger structure. Average kappa index values for cortical (0.97) and subcortical (0.91) structures demonstrated excellent agreement. To put these measures into perspective, a previous study demonstrated that a kappa index of 0.89 corresponded to an error of one pixel in the length of the long and short axes for a small structure such as the caudate on an image whose spatial resolution was 1 mm × 1 mm × 1 mm[22]. Therefore, the agreement demonstrated by using these mesh models was more than sufficient for knowledge-based brain structure segmentation. However, for shape analysis, any results with less than a pixel displacement could be due to the errors from the models themselves.

Our study was limited in several ways. First, for generality, an ideal brain atlas should be constructed from an average image of many subjects. We did construct average images from the images of 10 patients, and then aligned the images to the same pediatric template using the affine and nonlinear registration algorithm based on mutual information. Unfortunately, the sulci on these images, which were the major landmarks for manual delineation of brain structures, were too blurred to be clearly identified. Another approach we are currently investigating uses group registration, which aligns images to a group average space instead of to a previously defined template. Our study was also limited by details missing from our delineation of subcortical structures. Although we delineated them as carefully as possible, we

acknowledge that some details of subcortical structures were missing from the resulting brain atlas. An obvious example is the caudate illustrated in Figure 2. The lateral geniculate body and tail of the caudate are missing in the atlas. However, even with these limitations, no false positives were observed in the atlas.

In summary, we have constructed a digital pediatric brain atlas and its triangular mesh models for 25 cortical and subcortical brain structures, which are publicly available on the Internet (www.stjude.org/BrainAtlas). The atlas differs from previous brain atlases in that it was developed specifically for young children and in the fact that the WM has been roughly divided into WM associated with a specific lobe, WM that connects different regions, WM that interconnects two hemispheres, and WM that connects all lobes with subcortical structures. The atlas and its mesh models can be used in knowledge-based pediatric brain structure segmentation, shape analysis, and planning treatment.

ACKNOWLEDGEMENTS

This work is supported by Thrasher Research Fund awarded to Dr. Zuyao Shan and the Cancer Center Support Grant (CA21765) from the National Cancer Institute and by the American Lebanese Syrian Associated Charities (ALSAC).

REFERENCES

1. K. A. Ganser, H. Dickhaus, R. Metzner, and C. R. Wirtz, "A deformable digital brain atlas system according to Talairach and Tournoux", *Medical Image Analysis* **8**, pp. 3-22, 2004.
2. A. Pommert, M. Riemer, T. Schiemann, R. Schubert, U. Tiede, and K. H. Hohne, "Knowledge-Based and 3D Imaging-Systems in Medical-Education", *Information Processing '94, Vol Ii* **52**, pp. 525-532, 1994.
3. U. Tiede, M. Bomans, K. H. Hohne, A. Pommert, M. Riemer, T. Schiemann, R. Schubert, and W. Lierse, "A Computerized 3-Dimensional Atlas of the Human Skull and Brain", *American Journal of Neuroradiology* **14**, pp. 551-559, 1993.
4. K. H. Hohne, M. Bomans, M. Riemer, R. Schubert, U. Tiede, and W. Lierse, "A Volume-Based Anatomical Atlas", *IEEE Computer Graphics and Applications* **12**, pp. 72-78, 1992.
5. R. Kikinis, M. E. Shenton, D. V. Iosifescu, R. W. McCarley, P. Saiviroonporn, H. H. Hokama, A. Robatino, D. Metcalf, C. G. Wible, C. M. Portas, R. M. Donnino, and F. A. Jolesz, "A digital brain atlas for surgical planning, model-driven segmentation, and teaching", *Ieee Transactions on Visualization and Computer Graphics* **2**, pp. 232-241, 1996.
6. L. Thurfjell, C. Bohm, and E. Bengtsson, "Cba - An Atlas-Based Software Tool Used to Facilitate the Interpretation of Neuroimaging Data", *Computer Methods and Programs in Biomedicine* **47**, pp. 51-71, 1995.
7. M. M. Chakravarty, G. Bertrand, M. Descouteaux, A. F. Sadikot, and D. L. Collins, "The creation of a brain atlas for image guided neurosurgery using serial histological data", *Medical Image Computing and Computer-Assisted Intervention - Miccai 2003, Pt 1* **2878**, pp. 343-350, 2003.
8. D. Sutton, "The whole brain atlas", *British Medical Journal* **319**, p. 1507, 1999.
9. M. Y. Toh, R. B. Falk, and J. S. Main, "Interactive brain atlas with the visible human project data: Development methods and techniques", *Radiographics* **16**, pp. 1201-1206, 1996.
10. A. M. Rath, "Interactive brain atlas the digital anatomist", *Surgical and Radiologic Anatomy* **18**, p. 154, 1996.
11. M. Y. Toh, M. J. Ackerman, and J. Main, "Interactive Brain Atlas with the Visible-Human-Project Data", *Radiology* **197**, p. 533, 1995.
12. J. T. Huber, and N. B. Giuse, "Interactive Brain Atlas", *Journal of the American Medical Informatics Association* **2**, p. 294, 1995.
13. T. Paus, A. Zijdenbos, K. Worsley, D. L. Collins, J. Blumenthal, J. N. Giedd, J. L. Rapoport, and A. C. Evans, "Structural maturation of neural pathways in children and adolescents: In vivo study", *Science* **283**, pp. 1908-1911, 1999.
14. M. Wilke, V. J. Schmithorst, and S. K. Holland, "Normative pediatric brain data for spatial normalization and segmentation differs from standard adult data", *Magnetic Resonance in Medicine* **50**, pp. 749-757, 2003.
15. T. A. Woolsey, Hanaway J., and Gado M.H., *The brain atlas: a visual guide to human central Nervous system*, John Wiley & Sons, Inc., Hoboken, New Jersey, 2003.

16. M. B. Carpenter, *Core text of neuroanatomy*, Williams & Wilkins, Baltimore, MD, 1985.
17. Nolte J., *The human brain: an introduction to its functional anatomy*, Mosby Inc., St. Louis, 2002.
18. A. L. W. Bokde, S. J. Teipel, Y. Zebuhr, G. Leinsinger, L. Gootjes, R. Schwarz, K. Buerger, P. Scheltens, H. J. Moeller, and H. Hampel, "A new rapid landmark-based regional MRI segmentation method of the brain", *Journal of the Neurological Sciences* **194**, pp. 35-40, 2002.
19. J. J. Kim, B. Crespo-Facorro, N. C. Andreasen, D. S. O'Leary, B. Q. Zhang, G. Harris, and V. A. Magnotta, "An MRI-based parcellation method for the temporal lobe", *Neuroimage* **11**, pp. 271-288, 2000.
20. B. Crespo-Facorro, J. J. Kim, N. C. Andreasen, D. S. O'Leary, A. K. Wiser, J. M. Bailey, G. Harris, and V. A. Magnotta, "Human frontal cortex: An MRI-based parcellation method", *Neuroimage* **10**, pp. 500-519, 1999.
21. d. M. Berg, Kreveld van M., Overmars M., and Schwarzkopf O., *Computational geometry:algorithms and applications*, Springer-Verlag, Berlin, Germany, 2000.
22. B. M. Dawant, S. L. Hartmann, J. P. Thirion, F. Maes, D. Vandermeulen, and P. Demaerel, "Automatic 3-D segmentation of internal structures of the head in MR images using a combination of similarity and free-form transformations: Part I, Methodology and validation on normal subjects", *IEEE Trans. Med. Imaging* **18**, pp. 909-916, 1999.